Toward Reduced Transport Errors in a High Resolution CO_2 Inversion System

Aijun Deng[1], Thomas Lauvaux[1], Brian J. Gaudet[1], Natasha Miles[1], Kenneth J. Davis[1], Kai Wu[1], Daniel Sarmiento[1]
Kevin R. Gurney[2], Michael Hardesty[3], Tim Bonin[3] and Alan Brewer[3]
[1]The Pennsylvania State University, [2]Arizona State University, [3]NOAA Earth Science Research Laboratory

(18th Conference on Atmospheric Chemistry, 96th AMS Annual Meeting, 11-14 January 2016, New Orleans, LA)

Introduction

Atmospheric transport is one of the key components in estimating posterior surface fluxes using an atmospheric inversion system. We present here a real-time assimilation system applied to the Weather Research and Forecasting model (WRF) at high resolution to improve the representation of the atmospheric dynamics in the inversion system. In addition to utilizing an optimal model configuration in model physics, we continuously assimilate surface and low troposphere meteorological observations into the transport modeling system. For the Indianapolis Flux Experiment (INFLUX) project, we have developed a Four Dimensional Data Assimilation (FDDA) technique coupled to the WRF model and the high resolution CO_2 emission product Hestia to provide the most accurate transport solutions of the 3D fields of CO_2. Unlike intermittent data assimilation approaches (e.g., 3-D VAR, EnKF, etc) that introduce insertion noise detrimental to tracer transport applications, FDDA continuously and seamlessly assimilates observations at each model time step to produce dynamic analyses at a desired spatial resolution. It has been proven to be an effective method to constrain model error and is widely used in WRF modeling system (Deng et al. 2009, Rogers et al. 2013).

We evaluated the effect of assimilating various observations on the WRF solutions, and its impact on the linearized adjoint solutions used in the CO_2 inversion system for INFLUX. Since WMO upper-air observations are sparse in time (i.e., 12 hourly apart) and space (hundreds of kilometers apart), additional observations from different platforms were introduced, including the HALO lidar wind observations and aircraft measurements from the commercial airline program, Aircraft Communications Addressing and Reporting System (ACARS). We present the inverse CO_2 emissions over 2 months (September-October 2013) using different atmospheric simulations that assimilate surface stations, lidar, and ACARS, and assess the improvement in model performance based on the meteorological instrumentation used in our assimilation system.

Model Description

WRF Model Physics: 1) Single-Moment 5-class ice scheme microphysical processes (WSM5),
2) Kain-Fritsch scheme for cumulus parameterization on the 9-km grid,
3) RRTM for longwave atmospheric radiation, and the Dudhia scheme for shortwave atmospheric radiation,
4) Level 2.5 TKE-predicting MYNN turbulent closure scheme (MYNN PBL),
5) 4-layer unified Noah land surface processes.
6) WRF-Chem (Grell et al. 2005) V3.5.1 release is used here

Meteorological Data Assimilation: WRF FDDA with both analysis nudging and observation nudging (Deng et al. 2009, Rogers et al. 2013) are used. Using FDDA techniques, observations were assimilated continuously into the WRF-Chem system to produce a dynamic analysis, blending the model simulations and the observations to produce the most accurate meteorological conditions possible to simulate the atmospheric CO_2 concentrations in space and time over the Indianapolis region.

Data Types Assimilated: 1) Standard WMO surface and upper-air observations, available hourly for surface and 12-hourly for upper air.
2) Wind profiles from the local HALO lidar deployed by NOAA Earth System Research Laboratory Chemical Sciences Division (http://www.esrl.noaa.gov/csd/groups/csd3/measurements/influx/) at a location in Indianapolis, available at 20-min. intervals.
3) The Aircraft Communications Addressing and Reporting System (ACARS) commercial aircraft observations, available anywhere in space and time with low-level observations near the major airports.

Modeling System Configuration

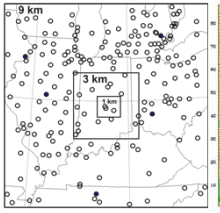

Figure 1. WRF 9/3/1-km grid configuration.

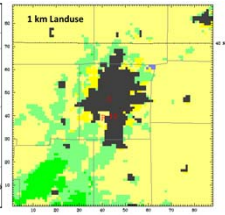

Figure 2. WRF 1-km grid landuse.

WRF Model Grids: *9km: 101x101, 3km: 100x100; 1km: 88x88;* Fifty nine (59) vertical terrain-following layers, with the first model layer at about 7 m AGL and with 24 model layers below 1.5 km AGL , Ptop=100 hPa, one-way nesting. Model grids with WMO station distribution, and the landuse for the 1-km grid are shown in Figs. 1 and 2.

Model Initialization: 3-hourly NARR analyses at 32x32-km resolution are used for the initial conditions and lateral boundary conditions (ICs/LBCs). The IC fields are further enhanced by rawinsonde and surface data through the WRF objective analysis process, Obsgrid, using a modified Cressman analysis method (Deng et al. 2009). The three-dimensional (3D) analyses and the surface analysis fields used for analysis FDDA are also enhanced by the objective analysis process and are defined at three-hour intervals. For the chemistry initialization with CO_2, Hestia 2012 product (Gurney et al. 2012) was used to determine the emission values .

FDDA Configuration: Multiscale FDDA with 3D analysis nudging and surface analysis nudging on the 9-km grid , and observation nudging of WMO obs on the 3– and 1-km grids. No mass field (temperature and moisture) observations are assimilated in PBL so that model physics are dominant.

Experimental Design

WRF-Chem system was configured to run for a two-month period (Sept.-Oct. 2013), in 5-day segments with a 12-hour overlapping time-window. The WRF model solutions are then used to drive a Lagrangian Particle Dispersion Model (LPDM) that calculates the CO_2 footprints of each CO_2 tower observations. The footprints are used to compute the influence function in the inversion system to compute the updated posterior CO_2 fluxes. Four different WRF configurations (or experiments) are conducted and results of both meteorological fields and posterior CO2 fluxes are compared among the four experiments:

NOFDDA : No data assimilation of any form is applied. WRF is run driven by NARR
FDDA_WMO: Only standard WMO surface and upper-air observations are assimilated.
FDDA_WMO_Lidar: In additional to WMO observations, wind profiles from the local HALO lidar are also assimilated.
FDDA_WMO_Lidar_ACARS: In addition to the WMO and lidar data, the ACARS observations are also assimilated .

Results

Table 1. Mean error (ME) and mean absolute error (MAE) of the WRF-predicted 10-m wind direction, wind speed and 2-m temperature over the 1-km grid verified hourly against three WMO surface measurements, averaged over the period between 00 UTC 27 August and 00 UTC 3 November 2013.

		NOFDDA	FDDA_WMO	FDDA_WMO_Lidar	FDDA_WMO_Lidar_ACARS
Wind Direction	ME	6	2	2	1
	MAE	30	19	19	19
Wind Speed	ME	0.2	0.1	0	-0.2
	MAE	1.0	0.8	0.8	0.8
Temperature	ME	-1.0	-0.8	-0.9	-1.4
	MAE	2.3	2.3	2.4	2.2

Table 2. Same as Table 1, except for the upper-air (below 2 km AGL) INFLUX lidar measurements (winds only) and ACARS measurements (winds and temperature).

		NOFDDA	FDDA_WMO	FDDA_WMO_Lidar	FDDA_WMO_Lidar_ACARS
Wind Direction	ME	4	2	-1	0
	MAE	26	24	15	14
Wind Speed	ME	0.2	-0.2	-0.2	-0.2
	MAE	2.0	2.0	1.3	1.2
Temperature	ME	0.8	1.0	1.0	0.5
	MAE	1.3	1.4	1.4	0.8

Table 3. Same as Table 1, except for the WRF-predicted PBL depth verified hourly against the Indianapolis INFLUX lidar measurements.

	NOFDDA	FDDA_WMO	FDDA_WMO_Lidar	FDDA_WMO_Lidar_ACARS
ME	25	103	83	-23
MAE	259	272	254	223

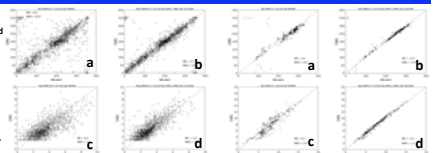

Figure 3. WRF-predicted versus observed wind direction (a: NOFDDA, b: FDDA_WMO_Lidar_ACARS), wind speed (c: NOFDDA, d: FDDA_WMO_Lidar_ACARS) and temperature (e: NOFDDA, f: FDDA_WMO_Lidar_ACARS) on the 1-km resolution grid, averaged over the time period between 00 UTC 27 August and 00 UTC 3 November 2013, comparing between NOFDDA (left) and FDDA_WMO_Lidar_ACARS (right) experiments. Each '+' represents the mean of meteorological variable of the three WMO surface stations at a given hour.

Figure 4. WRF-predicted versus observed wind direction (a: NOFDDA, b: FDDA_WMO_Lidar_ACARS), wind speed (c: NOFDDA, d: FDDA_WMO_Lidar_ACARS) and temperature (e: NOFDDA, f: FDDA_WMO_Lidar_ACARS) on the 1-km resolution grid, averaged over the time period between 00 UTC 27 August and 00 UTC 3 November 2013, comparing between NOFDDA (left) and FDDA_WMO_Lidar_ACARS (right) experiments. Each '+' represents the 5-day mean of meteorological variable over all the observations from INFLUX lidar and ACARS in a given vertical 100-m height zone.

Model error can be reduced by assimilating meteorological observations (Tables 1 and 2, Fig. 3 through 6). However, the assimilation of the WMO surface stations has a limited impact in the vertical (up to 900m max.). The assimilation of the wind profiles from the HALO lidar improved the WRF simulated wind speed and direction up to 2km high. The model performances were further increased due to the assimilation of ACARS data, filling the gaps between the 12-hourly WMO radiosondes and providing a better spatial density than the Lidar data. The model-predicted PBL depth is also improved indirectly by assimilating meteorological observations (Table 3 and Fig. 7).

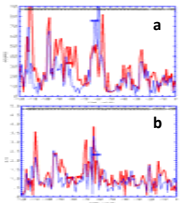

Figure 5. WRF error verified against the observations, for WRF wind direction (a) and wind speed (b) MAE time series comparing two experiments NOFDDA (red) and FDDA_WMO (blue), for the 1-km grid, for the 5-day simulation starting at 12 UTC 23 September 2013.

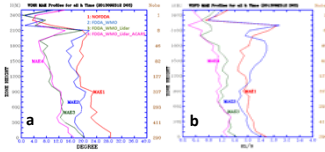

Figure 6. Model wind direction (a) and wind speed (b) MAE, comparing all four experiments: NOFDDA (MAE1), FDDA_WMO (MAE2), FDDA_WMO_Lidar (MAE3) and FDDA_WMO_Lidar_ACARS (MAE4), averaged over time for the 5-day simulation starting 12 UTC 23 September 2013, for the 1-km grid.

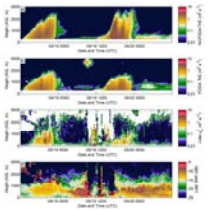

Figure 7. Comparison of PBL structures between WRF and the INFLUX lidar observations at Indianapolis for 28 and 30 August 2013: a) WRF-predicted TKE from Expt. NOFDDA, b) WRF-predicted TKE from Expt. FDDA_WMO_Lidar_ACARS, c) Lidar-observed vertical velocity variances, and d) Lidar-observed Signal-to-Noise Ratio (SNR).

The 5-day inverse emissions were computed using a Bayesian inversion system at 1-km resolution over the urban area of Indianapolis. Figure 8 shows the Observation network showing 12 INFLUX towers, and Figure 9 shows the results over the two-month period (Sept-Oct 2013) for the whole-city emissions. The variability among the 3 inversion cases represents the impact of differences in the WRF simulations. The WRF-FDDA with Lidar represents the optimal configuration with lower errors in both wind speed and direction, and is considered here as the reference case. Overall, the inverse emissions over the two months vary from 80ktC for Hestia to 90-95ktC for the different inversion estimates. The differences of about 50ktC among the inverse estimates represents about 50% of the change in the emissions compared to Hestia.

The Lagrangian Particle Dispersion Model (Uliasz 1994) was coupled to the WRF model over the two-months (Sept-Oct 2013). Particles were released continuously from the 12 tower locations in backward mode to simulate the area at the surface which directly influences the atmospheric concentrations. The footprints for 24 September 2013 are shown in Figure 10. The variability of the surface influence functions correspond to the differences in both wind speed (extent of the footprints along the main wind direction) and wind direction (width of the footprints). For this particular day, the wind direction varies only slightly between the three configurations whereas the wind speed was too high without the use of the FDDA system.

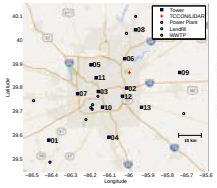

Figure 8. Observation network showing 12 INFLUX towers.

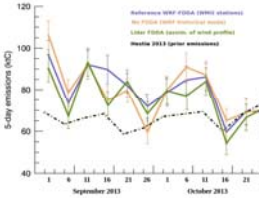

Figure 9. Five-day CO_2 emissions over Indianapolis using the three different WRF simulations. The Hestia CO_2 emissions were aggregated at 1km resolution and used as prior emissions in the inversion system (Gurney et al., 2012), indicated in black. The inverse emissions correspond to the 3 configurations described above with WRF in historical mode (NOFDDA, in orange), assimilating the WMO stations (FDDA-WMO, in purple), and assimilating the WMO and the HALO Lidar data (FDDA-WMO_Lidar, in green).

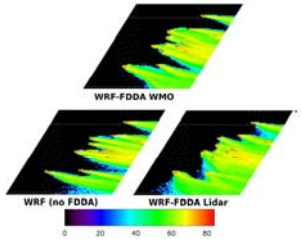

Figure 10. Influence functions over Indianapolis at 1km resolution for the 12 tower locations of the INFLUX network using the LPDM (Uliasz et al., 1994), for 24 September 2013 (aggregated over 17-22UTC) driven by the meteorological variables from the three different WRF configurations, in ppm_day/(g/m^2/hour).

Conclusion

To estimate the impact of the meteorological assimilation system used in the Penn State CO_2 inversion system, we conducted three WRF simulations for a two-month period, with various meteorological data assimilation strategies applied, including four numerical experiments: NOFDDA, FDDA_WMO, FDDA_WMO_Lidar, and FDDA_WMO_Lidar_ACARS. Model error can be significantly reduced by assimilating WMO observations. However, the assimilation of the WMO surface stations has a limited impact in the vertical (up to 900m max.). The assimilation of the wind profiles from the HALO lidar improved the WRF simulated wind speed and direction up to 2km high. The model performances were further increased thanks to the assimilation of ACARS data, filling the gaps between the 12-hourly WMO radiosondes and providing a better spatial density than the Lidar data. It was found that assimilating meteorological observations can indirectly improve the model-predicted PBL depth.

The inverse emissions from the three simulations are significantly impacted by the quality of transport simulations, with a difference of 50% in the emission correction after inversion depending on the transport simulations. The use of meteorological data improved the model performances and provided more robust CO_2 emissions at the city scale, reducing the systematic errors in the inverse emissions. Therefore, we highly recommend the use of meteorological assimilation systems for high resolution inversions to avoid the propagation of systematic errors from the transport model into the emission estimates.

References

Deng, A., D.R. Stauffer, B.J. Gaudet, J. Dudhia, J. Hacker, C. Bruyere, W. Wu, F. Vandenberghe, Y. Liu and A. Bourgeois, 2009: Update on WRF-ARW end-to-end multi-scale FDDA system, *10th Annual WRF Users' Workshop*, Boulder, CO, June 23, 14 pp.

Grell GA, SE Peckham, R Schmitz, and SA McKeen, G Frost, WC Skamarock, and B Eder. 2005. Fully coupled 'online' chemistry in the WRF model. *Atmos. Environ.*, 39:6957-6976.

Gurney, K. R., I. Razlivanov, Y. Song, Y. Zhou, B. Benes, M. Abdul-Massih, 2012: Quantification of fossil fuel CO2 emissions at the building/street scale for a large US city. Environmental Science & Technology, 2012; 120815073657007 DOI: 10.1021/es3011282

Rogers, R. E., A. Deng, D. R. Stauffer, B. J. Gaudet, Y. Jia, S. Soong, S. Tanrikulu, 2013: Application of the Weather Research and Forecasting Model for Air Quality Modeling in the San Francisco Bay Area. *J. Appl. Meteor.*, 52, 1953-1973.

Uliasz, M., 1994: Lagrangian particle modeling in mesoscale applications, in Environmental Modelling II, edited by P. Zanetti, pp. 71-102, Computational Mechanics Publications, Southampton.

Acknowledgment: This research is funded by the National Institute of Standards and Technology (NIST).